Journal of Materials Chemistry C

Accepted Manuscript

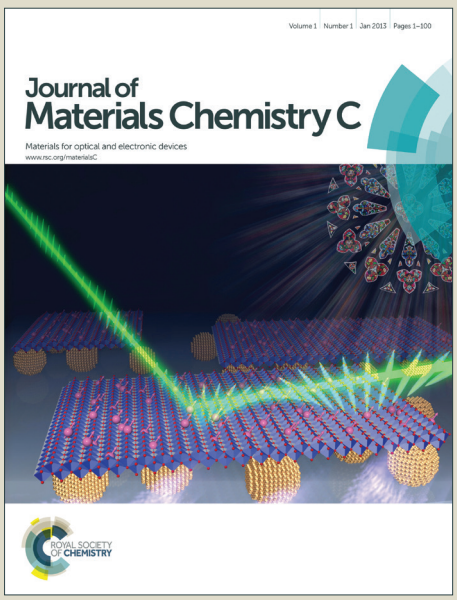

ROYAL SOCIETY OF CHEMISTRY

www.rsc.org/materialsC

Synthesis and Characterization of a Poly-Schiff Base with a Donor-acceptor Structure Containing Thiophene Units as Thermoelectric Materials†

Junjie Li, Chunhua Lai, Xiongzhi Xiang, Lei Wang*

Shenzhen Key Laboratory of Special Functional Materials, College of Materials Science and Engineering, Shenzhen University, Shenzhen 518060, China

Corresponding author: Lei Wang, Email address: wl@szu.edu.cn

Manuscript [to be] submitted to *Journal of Materials Chemistry C*

†Electronic supplementary information (ESI) available: The TGA curves, the FT-TR spectra of PSB(A) and its composites and SEM for inorganic fillers.

Abstract

As a representative conjugated polymer, the physical properties, such as electric conductivity and electro-optic properties, of poly-Schiff bases (PSB) have been widely investigated. However, to date, the thermoelectric (TE) properties of PSB or related polymers remain unreported. In this study, PSB with a donor-acceptor structure (PSB(A)) was synthesized and was blended with different fillers to prepare polymer-inorganic TE composites. For comparison, PSB with the common structure (PSB(B)) was also synthesized, and PSB(B)-graphite composites were fabricated. The PSB(A)/graphite composites exhibited a higher power factor of 10.2 $\mu Wm^{-1}K^{-2}$ compared with that of 4.5 $\mu Wm^{-1}K^{-2}$ for the PSB(B)/graphite composites at the same doping level. The effects of different fillers on the TE properties of the PSB(A)-based composites were investigated in detail, and the highest TE figure of merit, $ZT=2.53\times10^{-3}$, was obtained. The results show that the excellent TE materials could be produced by preparing polymer-inorganic TE composites using novel conducting polymers with a special structure (*e.g.,* donor-acceptor structure) and conducting fillers.

Keywords: Poly-Schiff base, Composite materials, Thermoelectric property, Conducting fillers

1. Introduction

The global demand for energy has risen dramatically, and the combustion of carbon-based fossil energy has caused serious environmental problems; therefore, many researchers have focused on affordable, renewable and clean energy resources along with sustainable energy conservation technologies over the past decades. As a possible means of energy conversion between heat and electricity without moving mechanical components or hazardous working fluids[1-3], TE materials have attracted a significant amount of attention. The energy conversion efficiency of TE devices is quantified by the dimensionless figure of merit, ZT, which is expressed as $ZT = S^2\sigma T/\kappa$, where S is the Seebeck coefficient, σ is the electrical conductivity, κ is the thermal conductivity, and T is the absolute temperature.

TE materials encompass a large family, including various materials, such as metal-based materials, ceramics, semiconductors and polymers. To date, the champion materials with high power factors are inorganic semiconductors and metal alloys, including Bi_2Te_3, SiGe, BiSb, $CoSb_3$, $CoAs_3$, $Cu_{2-x}Se$, and MgSi[4-6]. However, these inorganic materials with complex structures are prepared using the methods involving high-temperature, long-term and high-cost fabrication processes and have the problems of toxicity, poor processability, and low content in the earth[3, 4, 7]. Compared with inorganic TE materials, organic or polymer TE materials exhibit special inherent advantages, such as a potentially low cost because of the abundance of carbon resources, an overall simple synthesis, simple processing into versatile forms, high energy density, and low thermal conductivity, which may be of importance for their

TE applications[8, 9]. An additional advantage is that the physical and chemical properties of certain polymers are tunable over a relatively wide range of modifications by designing their molecular structures[10]. Among the polymer TE materials, increasing attention has recently been focused on conjugated polymers since the discovery of conducting polymers[11]. However, the low electrical conductivity (σ) and low Seebeck coefficient (S) of pure conjugated polymers have excluded them as feasible candidates for TE applications[12].

Fortunately, polymer-inorganic composites provide a promising method to synergistically combine the advantages of organic (low thermal conductivity) and inorganic (high σ) materials[13, 14]. AgNP (Ag nanoparticles)/polyaniline (PANI) nanocomposites[15] were prepared using a one-pot method and showed a maximum ZT of 5.73×10^{-5}. The CNT (carbon nanotubes)/PANI nanocomposites with a maximum power factor (5.04 $\mu Wm^{-1}K^{-2}$) were fabricated using a simple two-step method[16]. Paper-like single-walled carbon nanotubes (SWNT)/PANI composite films were prepared and exhibited good flexibility and enhanced TE properties[17]. Using a two-step spin casting method, poly(3,4-ethylenedioxythiophene):poly (styrenesulfonate) (PEDOT:PSS)/SWNT[18] with a layered structure was prepared and obtained a maximum power factor of 21.1 $\mu Wm^{-1}K^{-2}$. Composite films of poly(3-hexythiophene) and SWNT along with multi-walled carbon nanotubes (MWNT) with a competitive TE performance were obtained and showed a high ZT > 10^{-2} at room temperature[9]. (PEDOT:PSS)-coated MWNT with greatly enhanced TE property was prepared by Zhang and coworkers via a template-directed in situ

polymerization approach[19]. TE performances of PEDOT:PSS/expanded graphite films were investigated as a function of the graphite (G) concentration[20]. Nanocomposite 3D interconnected architecture consisting of reduced graphene (rGO) nanolayers sanwiched by polypyrrole (PPy) was obtained via an interfacial adsorption-soft template polymerization approach[21] and the highest power factor was 8.57 $\pm$0.76 $\mu Wm^{-1}K^{-2}$. Yoon *et al*. have reported an enhanced TE material of GNS (graphite nanosheets)/PVDF (poly(vinylidene fluoride)) composites[22].

According to the mentioned studies and other related reports[7, 14], the investigated polymer primarily focused on polyaniline (PANI), PPy , polythiophene (PTH) and their derivatives (PEDOT et al). To the best of our knowledge, as a representative conjugated polymer, the thermoelectric properties of the poly-Schiff base (PSB) or related polymers have not been previously investigated as TE materials. Additionally, although the various conducting materials, including silver (Ag), MWNT, SWNT and graphite (G), are reported as inorganic fillers, selecting the appropriate inorganic filler remains difficult because the properties of the materials have not been compared under the same filling conditions.

In this study, PSB with a donor-acceptor (D-A) structure was synthesized and was doped with different fillers (Ag, SWNT, MWNT and G) to prepare polymer-inorganic TE composites under the same filling conditions. Based on our previous studies[23-25], the weight contents of these fillers are designed as 40% and 80% in PSB(A)-based composites. The effects of these fillers on the TE properties of PSB(A)-based composites were investigated in detail. For comparison, PSB(B) was also synthesized,

and PSB(B)-G composites with G contents of 40 wt % and 80 wt % were fabricated.

2. Experimental Section

2.1 Materials

1-Naphthylamine (AR, 99%), p-phthalaldehyde (AR, 98%), p-phenylenediamine (AR, 97%), methanol (AR, 99.5%), iron(III) chloride hexahydrate (AR, 99%) and 2-thiophenecarboxaldehyde (98%) were purchased from Aladdin, Ltd and were used as received. Toluene was purchased from commercial sources and was dried with sodium wire prior to use. Zinc chloride, ethyl alcohol and p-toluene sulfonic acid were purchased from Tianjing Damao Chemical Reagent Co. Ltd and were used as received. Graphite was obtained from commercial sources with particle sizes over the 30 to 50 μm range, as measured by a laser particle size analyzer (Ls603). Layered-structure silver (Ag) was also obtained from commercial sources with sizes over the 2 to 5μm range, which was determined by scanning electron microscopy (SEM) (Fig.S1). Hydroxyl MWNT (Outer Diameter ＜ 8 nm, Inner Diameter = 2-5 nm, Length=10-30 μm) with a -OH content of 5.58 wt% and SWNT (Outer Diameter = 1-2 nm, Inner Diameter= 0.8-1.6 nm, Length =5-30 μm) with a -OH content of 3.96 wt% were purchased from Nanjing XFNANO Materials Tech Co., Ltd.

2.2 Preparation of poly[(2-(2-naphthalen-1-yl)vinyl)thiophene Schiff base] (PSB(A))

*2.2.1 Monomer synthesis ((2-(2-naphthalen-1-yl)vinyl)thiophene Schiff base)(*Ⅰ*)*

Into a three-neck round bottom flask equipped with a condenser, a nitrogen inlet-outlet, a Dean Stark trap and a magnetic stirrer, was introduced 1-naphthylamine (2.89 g, 0.02 mol), 2-thiophenecarboxaldehyde (1.88 mL, 0.02 mol), 0.01 g p-toluene sulfonic acid and 50 mL toluene. The polymerization reaction was vigorously stirred under a nitrogen atmosphere and heated at the reflux temperature for 10 h, while water was removed by azeotropic distillation with toluene. Then, the reaction mixture was cooled, and the solvent was removed under reduced pressure. A yellow powder was obtained with an overall yield of 60% after purification by recrystallization from ethyl alcohol.

^{1}H-NMR ($CDCl_3$, δ, ppm, $SiMe_4$as reference): 7.06-7.07 (d, 1H from the position 3 of thiophene, J=7.25 Hz), 7.15-7.17 (t, 1H from the position 4 of thiophene), 7.42-7.46 (t, 1H from the position 5 of thiophene), 7.49-7.56 (m, 4H from naphthyl), 7.70-7.72 (d, 1H from the position 5 of naphthyl, J=8.17 Hz), 7.82-7.85 (t, 1H from the position 4 of naphthyl), 8.34-8.36 (t, 1H from -CH=N-), 8.65 (s, 1H from the position 8 of naphthyl).

FTIR (powder). 1657 cm^{-1} (C=N stretching vibrations), 1601 cm^{-1} (C=C stretching vibrations), 776 cm^{-1} (out-of-plane C-H bending), 718 cm^{-1} (C-S bending vibrations).

2.2.2 Polymer synthesis

Monomer(**I**) (1.45 g, 0.006 mol) and 150 mL methanol were introduced into a 250 mL three-neck round bottom flask equipped with a condenser, a gas inlet-outlet and a magnetic stirrer. Then, 3.65 g (0.00135 mol) of iron (III) chloride hexahydrate was

added in portions over 30 min. A black color immediately appeared. The polymerization was performed for 24 h at 28 °C. The black colored product with a yield of 69% was separated by precipitation with deionized water, filtered through a Büchner funnel and then dried in a vacuum oven at 60 °C for 12 h.

2.3 Preparation of poly-Schiff base with the common structure (PSB(B))

P-phthalaldehyde (3.35 g, 25 mmol), p-phenylenediamine (2.7 g, 25 mmol), 50 mL toluene, 0.2 g zinc chloride and 0.1 g p-toluene sulfonic acid were added to a 250 mL, three-neck, round-bottom flask fitted with a Dean Stark trap, a magnetic stirrer, a condenser and a gas inlet-outlet. The mixture was vigorously stirred under a nitrogen atmosphere and heated to 130 °C for 1 h with a slow heating rate; the mixture was then maintained at the reflux temperature for 6 h, followed by precipitation and filtration using a Büchner funnel. The product was washed with deionized water until the filtrated fluid was colorless and was then washed with a portion of ethyl alcohol. Finally, the deep yellow product with an overall yield of 87.77% was dried in a vacuum oven at 80 °C for 12 h.

2.4 Preparation of Composites based on PSB(A) and PSB(B)

To promote mixing during the milling process, the PSB(A), PSB(B) and corresponding inorganic powders (G, Ag, MWNT, and SWNT) were combined with 200 mL anhydrous ethanol at different weight percent values (40 wt% and 80 wt%) and ultrasonicated for 30 min followed by mechanical blending at 1,500 rpm for

another 30 min. After filtering, the powder mixtures were dried at 60 °C for 24 h and then milled in an agate mortar for 1 h. Finally, the powder samples were milled in a 250 mL cylindrical steel jar with five 10 mm diameter steel balls and ten 5 mm diameter steel balls at a rotation speed of 270 rpm for 10 h.

2.5 Characterization

The morphologies of the bulk samples were observed using scanning electron microscopy (SEM, Hitachi S-4700). ^{1}H-NMR and ^{13}C-NMR spectra (Bruker AC FT-NMR spectrometor operating at 400MHz and 100MHz, respectively) were recorded at room temperature. The elemental analysis of samples were obtained using elemental analyzer (Vario, Elementar, German). The powdered samples were dispersed in KBr disks, and their Fourier transform infrared spectra (FT-IR) were recorded on a Fourier transform infrared spectrometer (IFS 120HR, Bruker). The phases of the composites were characterized by X-ray diffraction (XRD) using a Bruker D8 Advance X-ray diffractometer with Cu Kα radiation. Thermal gravimetric analysis (TGA) was conducted on a TGA-Q50 (USA) from room temperature to 600 °C at a heating rate of 10 °C min^{-1} under a nitrogen flow of 40 mL min^{-1} to examine the thermal stability of the materials. Raman spectra were collected using a Raman spectrometer (λ_{exc}=514.5 nm, RENISHAW, England). The electrical conductivities and Seebeck coefficients of the bulk composites were simultaneously measured using a Seebeck coefficient/electric conductivity measuring system (ZEM-2, ULVAC-RIKO, Japan) from 303 K to 393 K in a helium atmosphere. The thermal

conductivity was measured using a thermal conductivity tester (KY-DRX-RW, Shanghai). The cuboid specimen with dimensions of 16.0 mm × 5.10 mm × 3.0 mm was prepared under a pressure of 15 Mpa for the electrical properties measurement, and the disk specimen with a diameter of 15.0 mm and a height of 3.0-4.0 mm was prepared under a pressure of 20 Mpa for the thermal conductivity measurement.

3. Results and Discussion

3.1 Monomer and polymer synthesis

The synthetic route to monomer **I**, PSB(A) and PSB(B) is shown in Scheme 1. PSB(A) is a type of PSB with a D-A structure involving a naphthyl donor unit (electron-rich) and a thiophene acceptor unit (electron-deficient) separated by a C=N bond[26], while PSB(B) is a common-structure PSB. Monomer **I**, which has a Schiff base-type structure with thiophene and naphthyl groups, is highly soluble in organic solvents. It is well-known that the conducting polymer possessed disadvantages, including infusibility and insolubility in all of the known organic solvents[27] due to its rigid molecular chain and significant intermolecular forces. As members of the conducting polymers family, PSB(A) and PSB(B) also show the same properties. The solubility of PSB(A) has been improved due to the presence of the naphthyl group in the polymer chain[28], but it remains partially soluble in polar organic solvents (N,N-dimethylformamide, trichloromethane). Therefore, the chemical structures of PSB(A) and PSB(B) are difficult to confirm by ^{1}H-NMR and ^{13}C-NMR. In this study, the successful synthesis of monomer (**I**) was evidenced by FT-IR, elemental analysis,

^{1}H-NMR and ^{13}C-NMR, while the characterization of polymers A and B were recorded by elemental analysis and FT-IR , and the results are discussed below.

Elemental analysis of monomer **I**, PSB(A) and PSB(B) were carried out (Table 1). By comparing the measured chemical formula with the theoretic chemical formula, it can be seen that the synthesized monomer and polymers fit the structures of Scheme 1.

The ^{1}H-NMR spectrum of monomer I was obtained in deuterated trichloromethane. As shown in Fig. 1, the numbers of protons corresponding to each resonance based on integration of the resonances of the NMR spectrum are in good agreement with the proposed structure. The resonance peaks at 7.06-7.07, 7.15-7.17 and 7.42-7.46 ppm were assigned to the three different protons of the thiophene ring as labeled in Fig. 1. The peak at 8.34-8.36 ppm was attributed to the proton of -CH=N-[28]. The resonance peak at 8.65 ppm resulted from the proton at position 8 of naphthyl. The remaining peaks at 7.49-7.56, 7.70-7.72 and 7.82-7.85 were assigned to the six protons of naphthyl, which are clearly shown in Fig. 1.

The ^{13}C-NMR spectrum of monomer I obtained in deuterated trichloromethane is shown in Fig.2. The resonance peak at 153.06 ppm assigned to the carbon of -CH=N-[29]. There are fourteen other peaks in the corresponding region as would be expected. The number of resonance peaks (fifteen peaks) in the ^{13}C-NMR spectrum in conjunction with the ^{1}H-NMR spectrum, FT-IR and elemental analysis clearly confirm the proposed structure of monomer I.

The FT-IR spectra of PSB(A) and PSB(B) are shown in Fig. 3. A specific

characteristic of the IR spectrum of PSB(A) is the presence of less sharp peaks compared with the PSB(B) IR spectrum. Several low intensity peaks presented over the range of 2800-3000 cm^{-1} can be attributed to the C-H stretching vibrations[30]. The C=C stretching vibrations from the naphthyl ring present a band at 1609 cm^{-1} in the PSB(A) spectrum, while the same peak in the PSB(B) spectrum belongs to the benzene ring but shifted to 1611 cm^{-1} [31]. The peaks at 764-774 cm^{-1} from PSB(A) can be assigned to the superposition of the out-of-plane C-H bending of thiophene and the out-of-plane C-H bending from the ortho-disubstituted naphthalene ring[28]. For PSB(A), the peak at 715 cm^{-1} is characteristic of the C-S bending vibrations, which indicates the presence of a thiophene monomer[32]. For PSB(B), the peaks at 1,191 cm^{-1} and 847 cm^{-1} are attributed to the in-plane and out-of-plane aromatic C-H bending for the 1,4-disubstituted aromatic ring[33]. The C=N stretching vibrations in the PSB(A) and PSB(B) samples are identified at approximately 1654 cm^{-1} and 1693 cm^{-1}, respectively[28, 34], which demonstrate the successful synthesis of PSB(A) and PSB(B) under the applied conditions in agreement with the elemental analysis (Table 1).

3.2 TE performances of PSB(A)/G and PSB(B)/G composites

Fig. 4 and Fig. 5 show the Seebeck coefficients and power factors of the PSB(A)/G and PSB(B)/G composites at different temperatures, respectively. As shown in Fig. 4, the Seebeck coefficient of the PSB(A)/G composites with 40 wt% graphite was 23.1 μVK^{-1}, whereas the Seebeck coefficient for the PSB(B)/G composites at the same doping level was only 14.8 μVK^{-1} at 60 °C. As shown in Fig. 5, the resulting

PSB(A)/G composites exhibited a high power factor ($PF=S^2\sigma$) of 10.2 $\mu Wm^{-1}K^{-2}$ compared with that of 4.5 $\mu Wm^{-1}K^{-2}$ in the PSB(B)/G composites at 80% G content. A low bandgap polymer can be obtained by combining electron-rich (donor) and electron-deficient (acceptor) moieties in their repeating units[35, 36]. As discussed above, PSB(A) is a type of conjugated polymer with a D-A structure, which results in PSB(A) having a small band gap, and a conducting polymer with a small band gap facilitates doping to obtain intrinsic metallic conductivity. These internal D-A structures can also improve the charge carrier mobility because of the reduced interchain π-π stacking distance,[37, 38] and a higher Seebeck coefficient can be obtained by increasing the carrier mobility[25]. In conclusion, these differences in the Seebeck coefficients and power factors between the PSB(A)/G and PSB(B)/G composites are primarily ascribed to the special structure of PSB(A).

3.3 Characterizations of PSB(A)-related composites

The cross-sections of the bulk samples were obtained by quenching and fracturing. Fig. 6 shows representative SEM images of PSB(A) and its bulk composites, which reveal that all of these inorganic fillers were homogeneously dispersed within the PSB(A) matrix. In Fig. 6b, the polymer matrix appears as smooth objects, and G shows a flake-like morphology. Ag fillers appeared bright, while the polymer matrix appeared dark in the SEM images (Fig. 6c and 6d) because of the higher electron density of Ag compared with that of PSB(A)[39]. In addition, the layered structure of Ag can be observed in Fig.S1. In Fig. 6c and Fig. 6d, there are many voids in the polymer

matrix because of the poor affinity between PSB(A) and the Ag fillers[40]. In Fig. 6e and Fig. 6f, spaghetti-like slender SWNT and MWNT with a coil morphology are uniformly adhered on the surface of the polymer, and portions of the CNTs are coated by PSB(A). MWNT shows a larger diameter compared with that of SWNT. The CNTs in the samples prepared by our method were not aligned in the same direction.

TGA measurements were conducted under a nitrogen flow of 40mL min^{-1} from room temperature to 600 °C at a heating rate of 10 °C min^{-1}. The TGA results are shown in Fig. S2. PSB(A) and its composites exhibited good thermal stability. All of the composites showed a dramatic weight loss above 220 °C, which could be attributed to the decomposition of the PSB(A) powder. The weight loss also decreased as the content of inorganic filler increased. The enhancement of the thermal stability of these composites was ascribed to the improved interfacial interaction between the inorganic fillers and the polymer matrix[41]. Additionally, the high thermal stability and the uniform dispersion of fillers enhanced the thermal stability of the composites[42]. These results indicate that the TE properties of the composites could be studied below 200 °C without destroying the PSB(A) structure.

The XRD patterns of the as-synthesized PSB(A) and the as-prepared PSB(A)-based composites are shown in Fig. 7. The diffraction profile of PSB(A) shows one broad peak at approximately 20°, indicating a typical amorphous structure,[43] and the small sharp peak at approximately 30° demonstrated a low level of crystallinity. All of these characteristic peaks of the PSB(A)-related composites were attributed to the corresponding inorganic filler, and no new phases were observed, suggesting that no

chemical reaction occurred between the polymer and fillers. For example, in the XRD spectrum of the PSB(A)/80% G sample, prominent scattering at the Bragg angles of $2\theta = 26.6°$ and $2\theta = 55°$ were observed, which was attributed to G[44]. Another example is that these characteristic peaks belonging to Ag grew as the Ag concentration increased; however, the position of these peaks remained unchanged, which is shown in the spectra of the PSB(A)/40% Ag and PSB(A)/80% Ag composites.

FT-IR spectra of PSB(A) and its composites at room temperature are shown in Fig.S3. In Fig.S3, all of the samples show similar peaks over the wavenumbers ranging from 750 cm^{-1} to 1,600 cm^{-1}, which originates from the PSB(A), and the primary absorption peaks of PSB(A) were previously discussed (Fig. 3). These similar peaks demonstrate that the main-chain chemical structure of PSB(A) did not change during the blending procedure, which is in agreement with the XRD results. However, most of the absorption bands of PSB(A)-based composites exhibit different degrees of red-shifts compared with these peaks in the PSB(A) spectrum because of the physical interactions between the polymer matrix and inorganic fillers.

Raman spectra provide further evidence of the existence of strong physical interactions between PSB(A) and the inorganic fillers. Fig. 8 shows the Raman spectra for pure PSB(A) and the PSB(A)-related composites. For the pure PSB(A) powder, the primary types of stretching modes, including 1150 cm^{-1} (C-H bending vibration), 1,245 cm^{-1} (C-C inter-ring stretching), 1359 cm^{-1}(C-N stretching), 1492 cm^{-1} (C=C asymmetrical stretching), 1536 cm^{-1} (C=N stretching) and 1598 cm^{-1} (C-C stretching of the naphthalene ring), were displayed[45, 46]. The peaks of the C-N and

C-C stretching of the PSB(A)/40% MWNT, PSB(A)/40% SWNT and PSB(A)/40% G composites were shifted to lower frequencies compared with these peaks in the PSB(A) spectrum. For example, the band position for C-C stretching shifted from 1598 cm^{-1} for PSB(A) to 1575 cm^{-1} for PSB(A)/40%SWNT. According to previous Raman spectroscopic studies, strong π-π interactions exist between PSB(A) and these fillers (G,SWNT,MWNT)[8, 46]. A shift in the peaks of the PSB(A)/80%Ag composite related to C-N and C-C stretching was also observed, which revealed strong interactions between the polymer and the layered structure Ag (Fig.S1).[15, 47] In addition, the interactions were weaker than the π-π interactions because of a smaller red shift, as shown in Fig. 8.

3.4 TE performance of composites based on PSB(A)

The electrical conductivity of the prepared PSB(A)-related composites is shown in Fig. 9, and the Seebeck coefficient as a function of the inorganic fillers in the PSB(A)-based composites is shown in Fig. 10. It is clear that a higher weight ratio of inorganic fillers yields a higher electrical conductivity but a lower Seebeck coefficient, which revealed the trade-off relationship between the electrical conductivity and the Seebeck coefficient[48]. As mentioned, strong interactions between PSB(A) and these fillers exist, which can act as a bridge facilitating the hopping transport of carriers between the polymer and fillers[46], increasing the electrical conductivity.

As shown in Fig. 9, the PSB(A)/80% Ag sample showed the highest conductivity (50,761 S/m) compared with the other PSB(A)-based composites, including PSB(A)

/80% G (24450 S/m), PSB(A)/80% MWNT (854.7 S/m) and PSB(A)/80% SWNT (1880 S/m), at the same doping level and the same temperature (120 °C). The poor conductivity of the PSB(A)/MWNT and PSB(A)/SWNT composites was attributed to the CNTs in these samples prepared by our method, which showed an unordered arrangement morphology (Fig. 6e and Fig. 6f), and CNTs purchased from the commercial resource showed inferior electrical conductivity compared with G and Ag. For the PSB(A)/40% Ag sample, the Ag particles possess the highest density compared with other fillers (G,MWNT, and SWNT), resulting in a low volume ratio of Ag to PSB(A) in the composite. Hence, Ag fillers in the specimen were separated by the polymer without forming a conductive network (Fig. 6c), which indicated that the content of Ag fillers (40 wt%) is lower than the conductivity percolation threshold[49]. Simultaneously, these voids (Fig. 6c) in the matrix were harmful for enhancing the electrical conductivity. Thus, the sample containing 40wt% Ag, which possessed a high resistance beyond the measuring range of the test equipment ZEM-2，was not examined.

As shown in Fig. 10, the highest Seebeck coefficient (40.7 S/m) of the PSB(A)/40% SWNT composite at 120 °C was obtained. The PSB(A)/MWNT and PSB(A)/SMNT samples exhibited a relatively high Seebeck coefficient compared with the other PSB(A)-related composites, possibly because of the increased number of interfaces between the CNTs and the polymer. Additionally, CNTs with surface treatment can easily disperse in the polymer matrix and produce a higher Seebeck coefficient by increasing the contact between the filler and matrix[50]. In contrast, the poorest Seebeck

coefficient of the PSB(A)/80% Ag sample could be attribute to the least number of interfaces between filler and matrix and also the poor Seebeck coefficient of the metal. However, for all of these specimens, the increasing weight ratio of fillers enhanced the carrier concentration of these composites, which leads to a decrease in the Seebeck coefficient because of the decrease in the energy gap between the average electron energy and the Fermi level[51].

The thermal conductivity of the as-prepared PSB(A)-based composites at room temperature was measured using a KY-DRX-RW thermal conductivity tester. Although an increase in the thermal conductivity was observed with the addition of inorganic fillers in the matrix, the thermal conductivity value remained at a low level, even at a high concentration (80 wt%) of fillers, as shown in Fig. 11. The relatively low thermal conductivity of the PSB(A)/SWNT and PSB(A)/MWNT composites was primarily ascribed to the higher interface density (the interfacial area per unit volume) between the polymer and the CNTs compared with the PSB(A)/G composites[16] because the reduction of the thermal conductivity was dominated by the phonon-interface scattering, and a high interface density could scatter phonons more effectively, resulting in a lower thermal conductivity[51]. The Ag particles possess a highest density compared with other fillers, causing a low volume ratio of Ag to PSB(A) in the PSB(A)/Ag composites. Therefore, compared with the other fillers, the Ag fillers are the most easily buried in the polymer matrix, and the fillers are surrounded by significantly more polymer molecules. In addition, the voids (Fig. 6d) aided the decrease in the thermal conductivity. All of these factors would decrease the

thermal conductivity and result in the lowest thermal conductivity (0.333 W K^{-1} m^{-1}) for the PSB(A)/80% Ag sample.

Based on these measurements, Fig. 12 shows the power factors of the PSB(A)-based composites, and Fig. 13 compares the ZT values of the various samples as a function of different inorganic fillers at different temperatures. The relatively poor power factors ($PF=S^2\sigma$) of the PSB(A)/MWNT and PSB(A)/SWNT composites were ascribed to the relatively low electrical conductivity, while the poorest Seebeck coefficient should be responsible for the poor PF of the PSB(A)/80% Ag sample. By balancing the electrical conductivity and the Seebeck coefficient, the PSB(A)/80% G sample showed the highest PF (10.2 $\mu Wm^{-1}K^{-2}$) and the highest ZT value (2.53×10^{-3}) at 90 °C.

4. Conclusions

PSB with a donor-acceptor structure (A) and PSB with the common structure (B) were synthesized, and then polymer-inorganic TE composites were prepared. The resulting PSB(A)-G composites exhibited a high power factor of 10.2 $\mu Wm^{-1}K^{-2}$ compared with that of 4.5 $\mu Wm^{-1}K^{-2}$ for the PSB(B)-G composites at 80% G content. The effects of different fillers on the TE properties of the PSB(A)-based composites prepared by mechanical ball milling and cold pressing were investigated in detail, and the highest TE figure of merit, $ZT=2.53\times10^{-3}$, was obtained. The strategy of synthesizing novel conducting polymers with a special structure and then preparing organic-inorganic composites may emerge as a promising method to obtain

high-performance, large area, and flexible polymer TE materials.

Acknowledgements

The authors would like to thank the National Nature Science Foundation of China (Nos. 51003060, 51171117 and 51101103) and the Shenzhen Sci and Tech research grant (JC2011042 100070A and ZYC201105170225A) for their financial support.

References and Notes

1. T. M. Tritt and M. A. Subramanian, *Mrs Bull*, 2006, **31**, 188-194.
2. G. J. Snyder and E. S. Toberer, *Nat Mater*, 2008, **7**, 105-114.
3. M. He, F. Qiu and Z. Lin, *Energy Environ.Sci*, 2013, **6**, 1352-1361.
4. S. B. Han, W. T. Zhai, G. M. Chen and X. Wang, *Rsc Adv*, 2014, **4**, 29281-29285.
5. D. L. Zhao and G. Tan, *Appl Therm Eng*, 2014, **66**, 15-24.
6. H. Liu, X. Shi, F. Xu, L. Zhang, W. Zhang, L. Chen, Q. Li, C. Uher, T. Day and G. J. Snyder, *Nat Mater*, 2012, **11**, 422-425.
7. Y. Du, S. Z. Shen, K. F. Cai and P. S. Casey, *Prog.Polym.Sci*, 2012, **37**, 820-841.
8. K. L. Xu, G. M. Chen and D. Qiu, *J Mater Chem A*, 2013, **1**, 12395-12399.
9. C. Bounioux, P. Diaz-Chao, M. Campoy-Quiles, M. S. Martin-Gonzalez, A. R. Goni, R. Yerushalmi-Rozene and C. Muller, *Energy Environ.Sci*, 2013, **6**,

918-925.

10. R. R. Yue and J. K. Xu, *Synthetic Met*, 2012, **162**, 912-917.

11. H. Shirakawa, E. J. Louis, A. G. Macdiarmid, C. K. Chiang and A. J. Heeger, *J Chem Soc Chem Comm*, 1977, 578-580.

12. Q. Yao, Q. Wang, L. M. Wang, Y. Wang, J. Sun, H. R. Zeng, Z. Y. Jin, X. L. Huang and L. D. Chen, *J Mater Chem A*, 2014, **2**, 2634-2640.

13. M. H. Elsheikh, D. A. Shnawah, M. F. M. Sabri, S. B. M. Said, M. H. Hassan, M. B. A. Bashir and M. Mohamad, *Renew Sust Energ Rev*, 2014, **30**, 337-355.

14. N. Dubey and M. Leclerc, *J Polym Sci Pol Phys*, 2011, **49**, 467-475.

15. W. J. Wang, S. P. Sun, S. J. Gu, H. W. Shen, Q. H. Zhang, J. J. Zhu, L. J. Wang and W. Jiang, *Rsc Adv*, 2014, **4**, 26810-26816.

16. C. Z. Meng, C. H. Liu and S. S. Fan, *Adv Mater*, 2010, **22**, 535-539.

17. J. L. Liu, J. Sun and L. Gao, *Nanoscale*, 2011, **3**, 3616-3619.

18. H. J. Song, C. C. Liu, J. K. Xu, Q. L. Jiang and H. Shi, *Rsc Adv*, 2013, **3**, 22065-22071.

19. Z. Zhang, G. Chen, H. Wang and X. Li, *Chem-Asian J*, 2015, **10**, 149-153.

20. M. Culebras, C. M. Gomez and A. Cantarero, *J Mater Sci*, 2013, **48**, 2855-2860.

21. G. Chen, Z. Zhang, W. Zhai and h. wang, *J Mater Chem C*, 2015, DOI: 10.1039/C4TC02471K.

22. H. D. Yoon, S. Nam, N. D. K. Tu, D. Kim and H. Kim, *Polym-Korea*, 2013, **37**, 638-641.

23. L. Wang, X. L. Jia, D. G. Wang, G. M. Zhu and J. Q. Li, *Synthetic Met*, 2013, **181**, 79-85.

24. L. Wang, D. G. Wang, G. M. Zhu, J. Q. Li and F. Pan, *Mater Lett*, 2011, **65**, 1086-1088.

25. J. Li, L. Wang, X. Jia, X. Xiang, C.-L. Ho, W.-Y. Wong and H. Li, *Rsc Adv*, 2014, **4**, 62096-62104.

26. W. G. Skene and S. Dufresne, *Org Lett*, 2004, **6**, 2949-2952.

27. C. I. Simionescu, M. Grigoras, I. Cianga, I. Diaconu and A. Farcas, *Polym Bull*, 1994, **32**, 257-264.

28. C. I. Simionescu, M. Grigoras, I. Cianga and N. Olaru, *Eur Polym J*, 1998, **34**, 891-898.

29. M. Kamaci and I. Kaya, *Polym Eng Sci*, 2014, **54**, 1664-1674.

30. Y. D. Wang and M. F. Rubner, *Synthetic Met*, 1990, **39**, 153-175.

31. M. R. Karim, J. H. Yeum, M. S. Lee and K. T. Lim, *Mater Chem Phys*, 2008, **112**, 779-782.

32. Y. A. Udum, K. Pekmez and A. Yildiz, *Eur Polym J*, 2005, **41**, 1136-1142.

33. X. R. Zeng and T. M. Ko, *Polymer*, 1998, **39**, 1187-1195.

34. X. C. Li, C. S. Li and S. J. Li, *Synthetic Met*, 1993, **60**, 285-288.

35. H. Hoppe and N. S. Sariciftci, *J Mater Res*, 2004, **19**, 1924-1945.

36. R. Gaudiana and C. Brabec, *Nat Photonics*, 2008, **2**, 287-289.

37. L. Burgi, M. Turbiez, R. Pfeiffer, F. Bienewald, H. J. Kirner and C. Winnewisser, *Adv Mater*, 2008, **20**, 2217-2224.

38. T. Umeyama, Y. Watanabe, M. Oodoi, D. Evgenia, T. Shishido and H. Imahori, *J Mater Chem*, 2012, **22**, 24394-24402.

39. L. Zhao, X. C. Pang, R. Adhikary, J. W. Petrich, M. Jeffries-EL and Z. Q. Lin, *Adv Mater*, 2011, **23**, 2844-2849.

40. D. Kim, Y. Kim, K. Choi, J. C. Grunlan and C. H. Yu, *Acs Nano*, 2010, **4**, 513-523.

41. S. T. Huxtable, D. G. Cahill, S. Shenogin, L. P. Xue, R. Ozisik, P. Barone, M. Usrey, M. S. Strano, G. Siddons, M. Shim and P. Keblinski, *Nat Mater*, 2003, **2**, 731-734.

42. G. X. Chen, H. S. Kim, B. H. Park and J. S. Yoon, *Polymer*, 2006, **47**, 4760-4767.

43. J. J. Li, X. F. Tang, H. Li, Y. G. Yan and Q. J. Zhang, *Synthetic Met*, 2010, **160**, 1153-1158.

44. Z. D. Han and J. Q. Wang, *Chin. J. Inorg. Chem*, 2003, **19**, 1366-1370.

45. S. Garreau, G. Louarn, J. P. Buisson, G. Froyer and S. Lefrant, *Macromolecules*, 1999, **32**, 6807-6812.

46. L. M. Wang, Q. Yao, H. Bi, F. Q. Huang, Q. Wang and L. D. Chen, *J Mater Chem A*, 2014, **2**, 11107-11113.

47. H. L. Lu, H. Xu, Y. Chen, J. L. Zhang and J. X. Zhuang, *Rsc Adv*, 2014, **4**, 5873-5879.

48. M. He, F. Qiu and Z. Lin, *Energy Environ.Sci*, 2013, **6**, 1352-1361.

49. Q. M. Jia, J. B. Li, L. F. Wang, J. W. Zhu and M. Zheng, *Mat Sci Eng a-Struct*,

2007, **448**, 356-360.

50. S. Y. Mun, H. M. Lim, H. Ahn and D. J. Lee, *Macromol Res*, 2014, **22**, 613-617.

51. M. He, J. Ge, Z. Q. Lin, X. H. Feng, X. W. Wang, H. B. Lu, Y. L. Yang and F. Qiu, *Energy Environ.Sci*, 2012, **5**, 8351-8358.

Figure Captions

Table 1 Elemental analysis results of monomer **I**, PSB(A) and PSB(B)

Scheme 1 Synthesis of PSB(A) and PSB(B) and schematic representation of monomer **I**

Fig. 1 ^{1}H-NMR spectrum of monomer **I**

Fig. 2 ^{13}C-NMR spectrum of monomer **I** in $CDCl_3$

Fig. 3 FT-IR spectra of PSB(A) and PSB(B) powders

Fig. 4 Seebeck coefficients for the PSB(A)/G and PSB(B)/G composites at 40 wt % and 80 wt % graphite contents

Fig. 5 Power factors for the PSB(A)/G and PSB(B)/G composites at 40 wt % and 80 wt % graphite contents

Fig. 6 Representative SEM images of cross-sections for the prepared samples:(a) pure PSB(A), (b) A/40%G, (c) A/40%Ag, (d) A/80%Ag, (e) A/80%SWNT, (f) A/80%MWNT

Fig. 7 X-ray diffraction patterns of PSB(A) and its composites. The inset shows the X-ray diffraction patterns for PSB(A).

Fig. 8 Raman spectra for PSB(A) and PSB(A)-based composites

Fig. 9 Electrical conductivities of PSB(A)-based composites (a,b)

Fig. 10 Seebeck coefficients of PSB(A)-based composites with 40 wt % and 80 wt % organic filler contents

Fig. 11 Thermal conductivities as a function of different inorganic fillers in the PSB(A)-based composites

Fig. 12 The correlation between power factors and inorganic fillers in PSB(A)-based composites at different temperatures

Fig. 13 ZT values of the PSB(A)-based composites at different temperatures

Table 1 Elemental analysis results of monomer **I**, PSB(A) and PSB(B)

Polymer	C (%)	H (%)	N (%)	S (%)	Measured formula	Theoretic formula
Monomer(**I**)	75.72	4.70	5.84	13.42	$C_{15.0}H_{11.1}N_{1.0}S_{1.0}$	$C_{15}H_{11}NS$
PSB(A)	75.75	3.87	5.98	11.74	$(C_{15.0}H_{9.2}N_{1.0}S_{0.9})_n$	$(C_{15}H_9NS)_n$
PSB(B)	79.93	4.89	13.32	–	$(C_{14.0}H_{10.3}N_{2.0})_n$	$(C_{14}H_{10}N_2)_n$

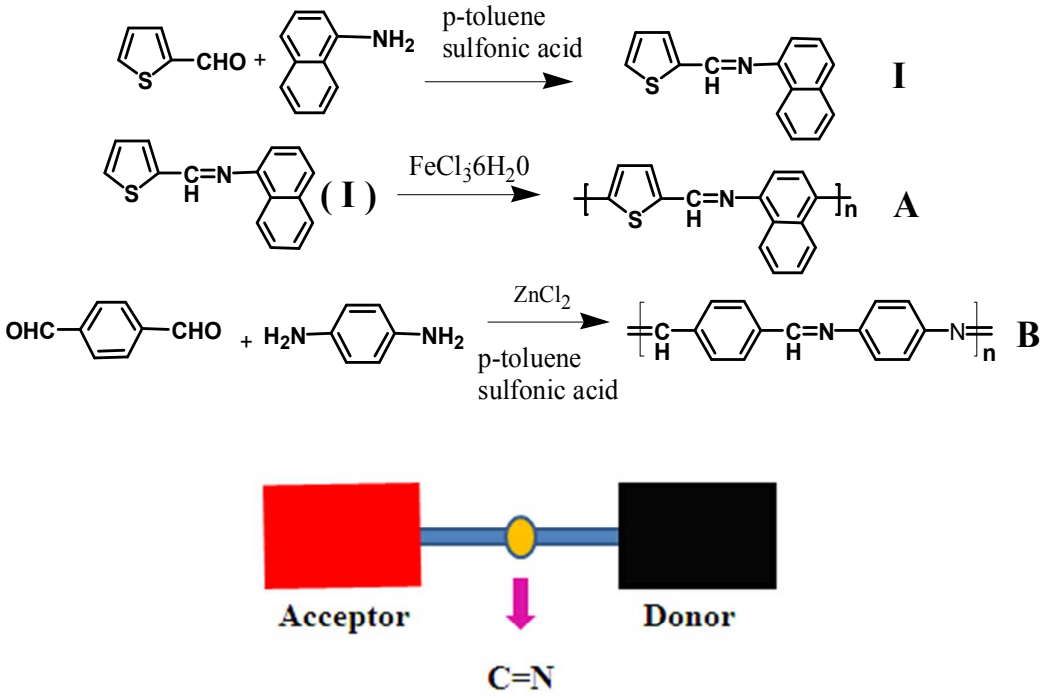

Scheme 1 Synthesis of PSB(A) and PSB(B) and schematic representation of monomer **I**

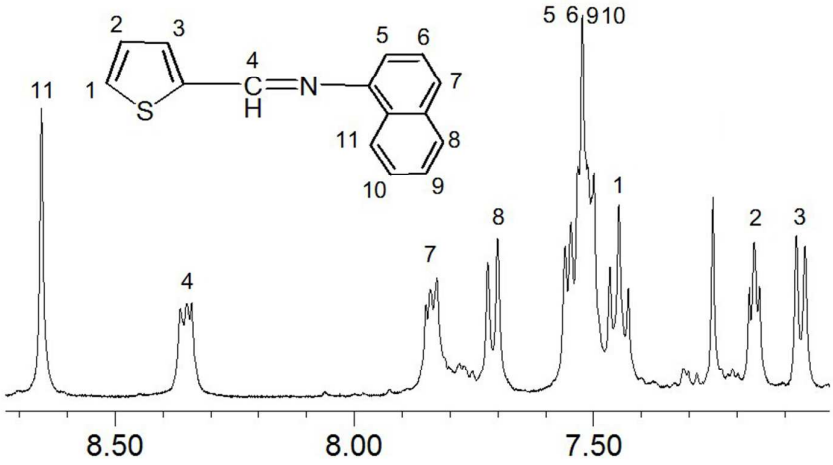

Fig. 1 ^{1}H-NMR spectrum of monomer **I**

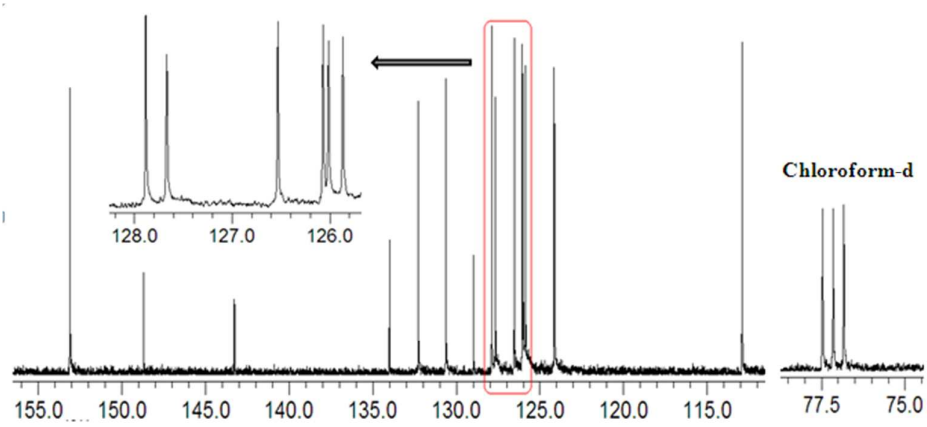

Fig. 2 ^{13}C-NMR spectrum of monomer **I** in $CDCl_3$

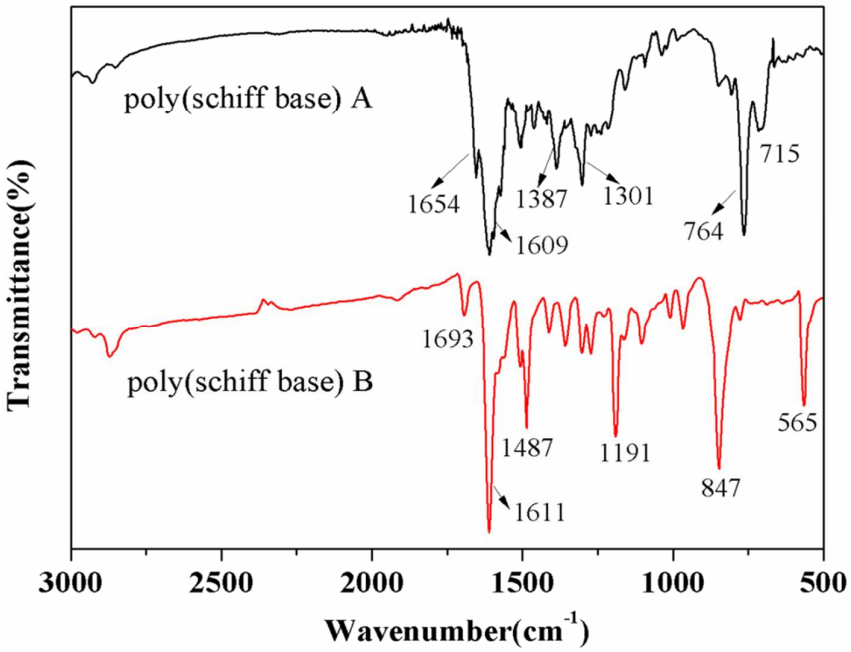

Fig. 3 FT-IR spectra of PSB(A) and PSB(B) powders

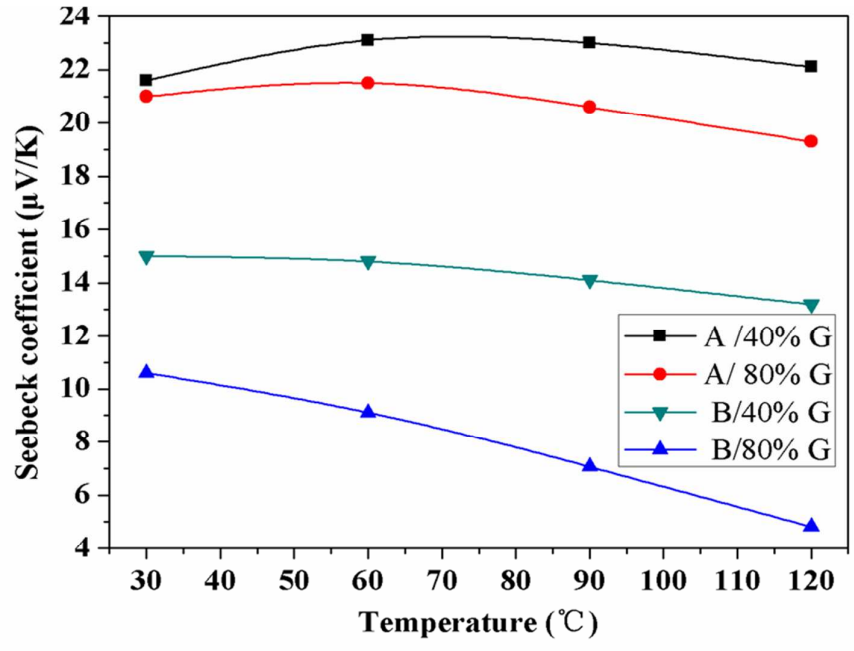

Fig. 4 Seebeck coefficients for PSB(A)/G and PSB(B)/G composites at 40 wt % and 80 wt % graphite contents

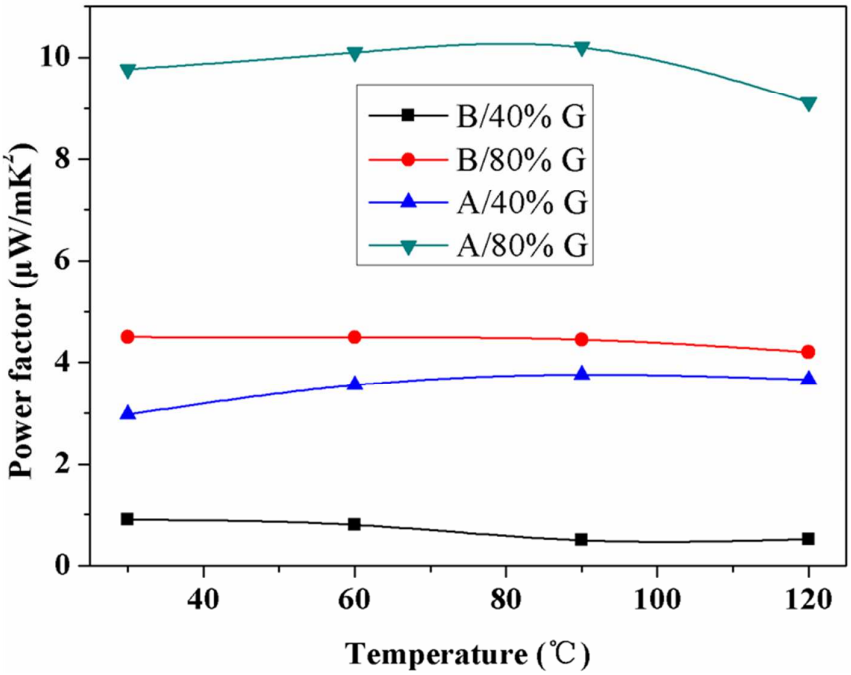

Fig. 5 Power factors for PSB(A)/G and PSB(B)/G composites at 40 wt % and 80 wt % graphite contents

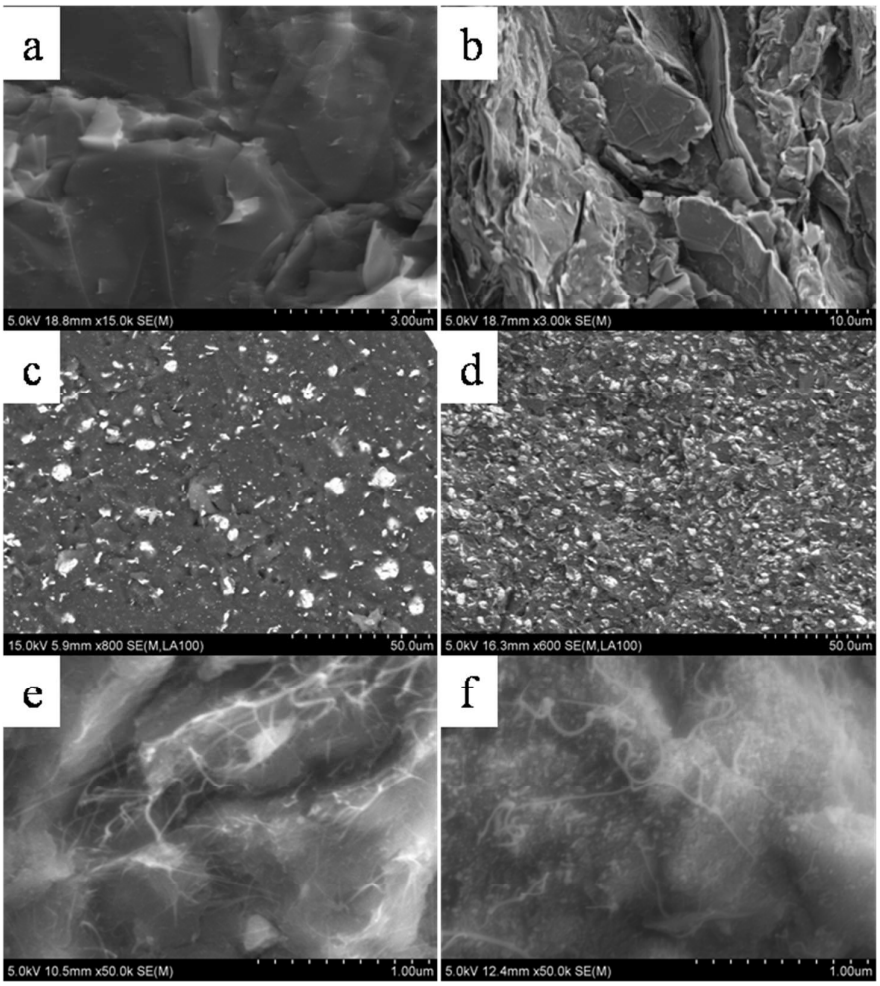

Fig. 6 Representative SEM images of cross-sections for the prepared samples:(a) pure PSB(A), (b) A/40%G, (c)A/40%Ag, (d)A/80%Ag, (e)A/80%SWNT, (f)A/80%MWNT

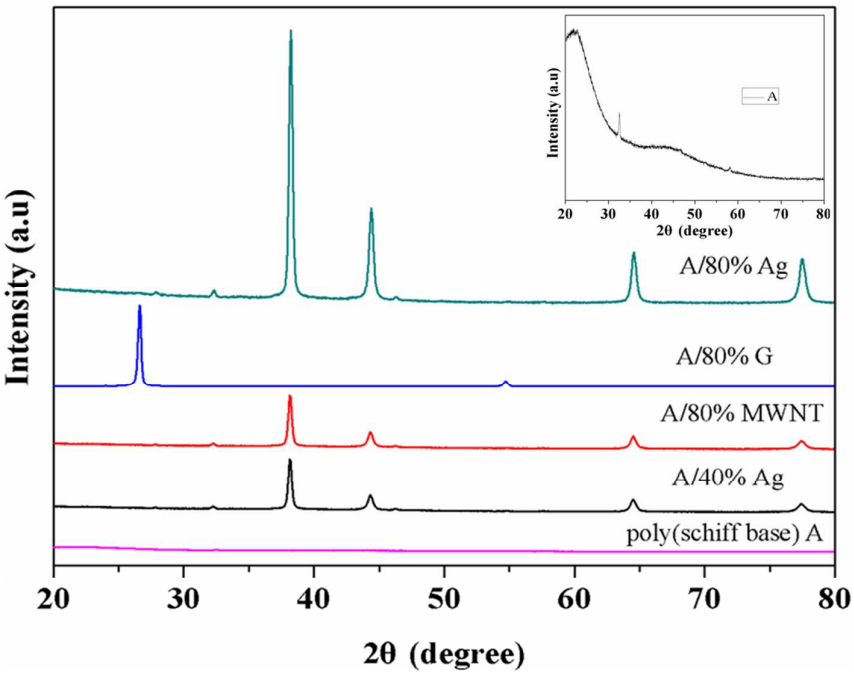

Fig. 7 X-ray diffraction patterns of PSB(A) and its composites. The inset shows the X-ray diffraction patterns for PSB(A).

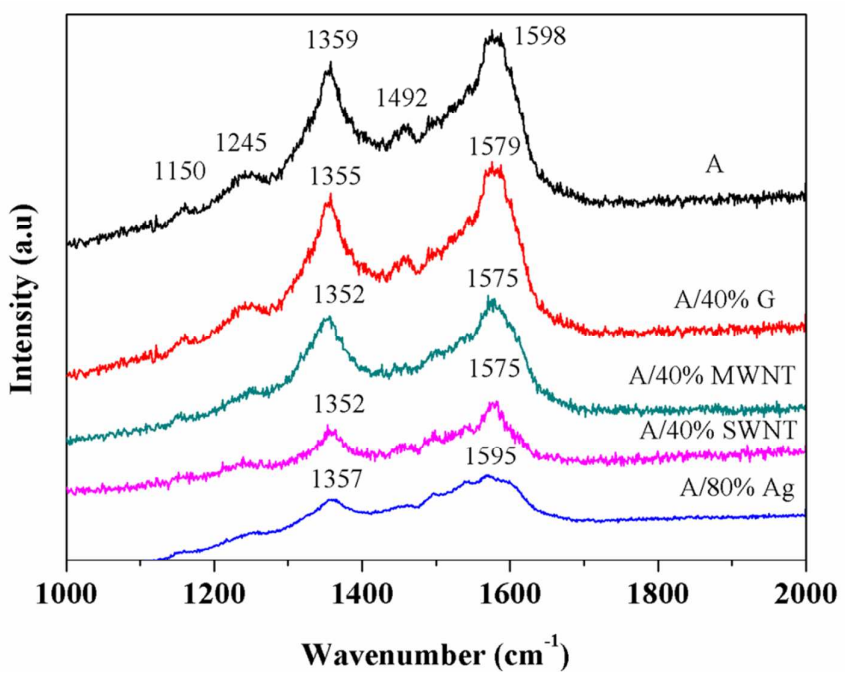

Fig. 8 Raman spectra for PSB(A) and PSB(A)-based composites

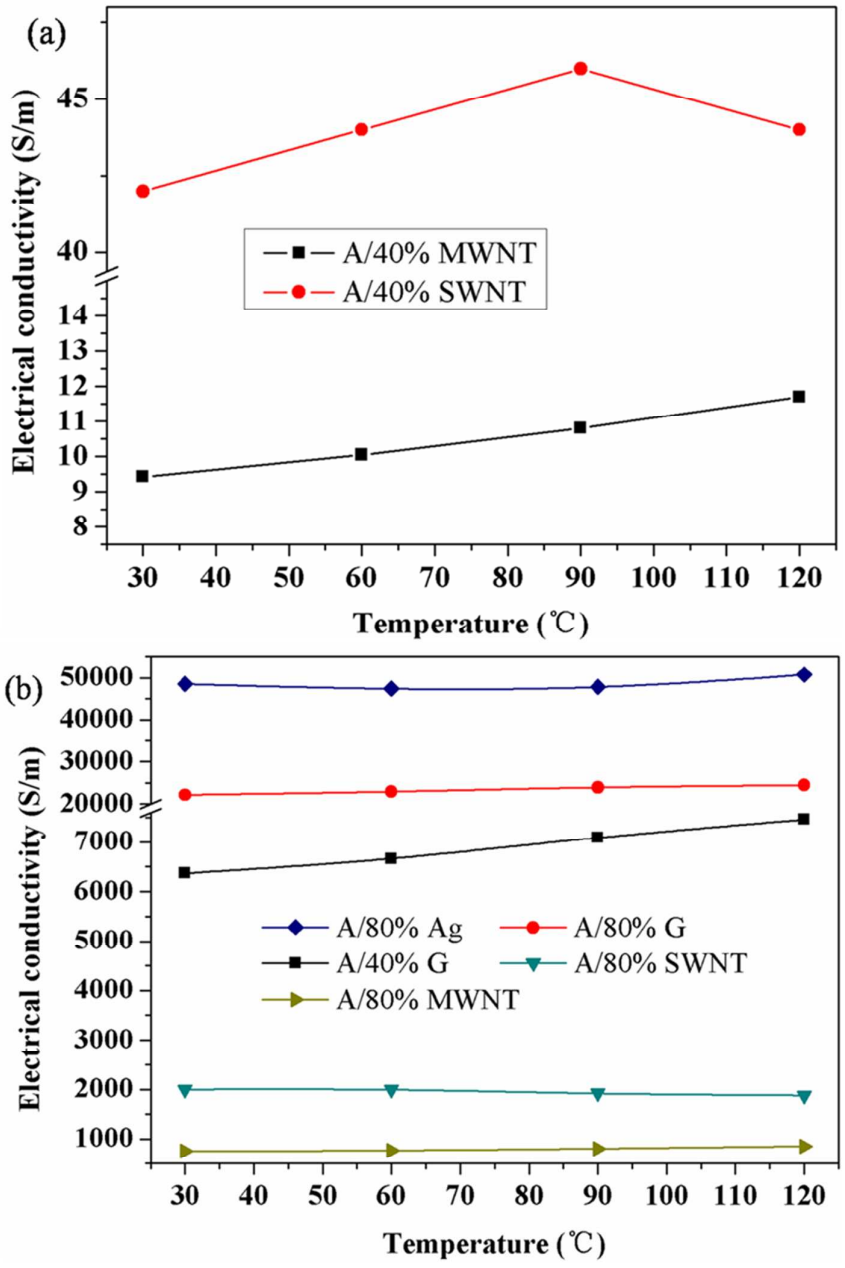

Fig. 9 Electrical conductivities of PSB(A)-based composites (a,b)

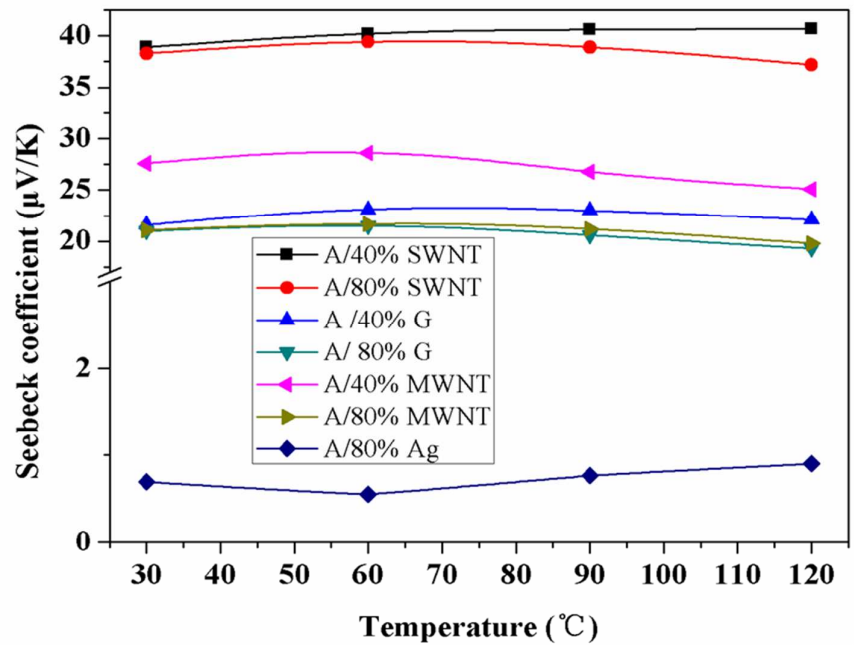

Fig. 10 Seebeck coefficients of PSB(A)-based composites with 40 wt % and 80 wt % organic filler contents

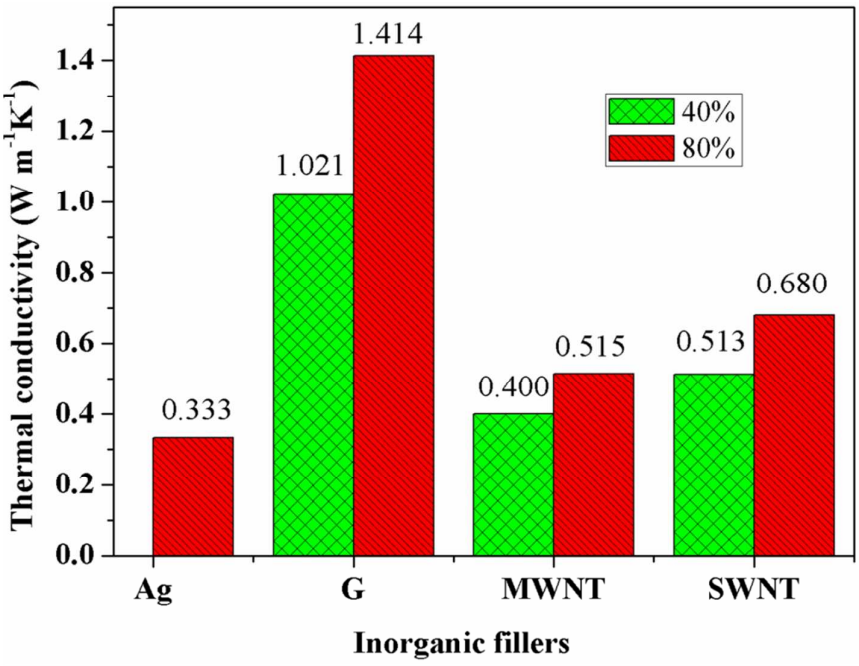

Fig. 11 Thermal conductivities as a function of different inorganic fillers in PSB(A)-based composites

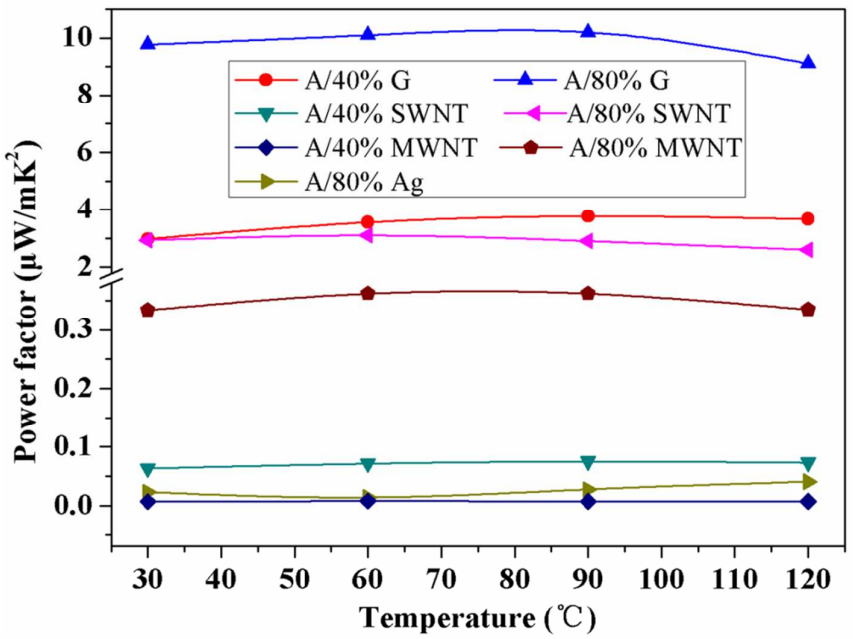

Fig. 12 The correlationbetweenpower factors and inorganic fillers in PSB(A)-based composites at different temperatures

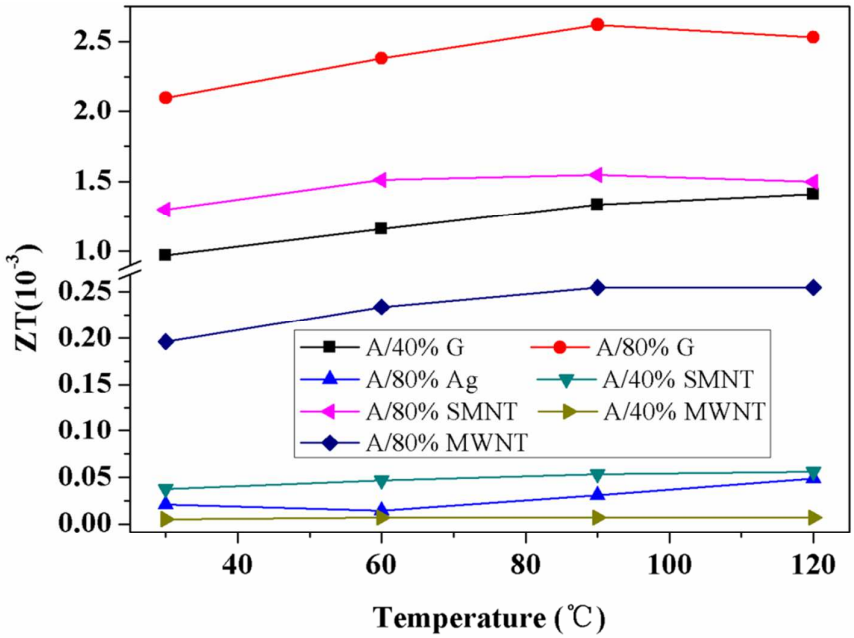

Fig. 13 ZT values of PSB(A)-based composites at different temperatures